Stress Tensor Eigenvector Following with Next-Generation Quantum Theory of Atoms in Molecules: Excited State Photochemical Reaction Path from Benzene to Benzvalene

Stress Tensor Eigenvector Following with Next-Generation Quantum Theory of Atoms in Molecules: Excited State Photochemical Reaction Path from Benzene to Benzvalene

Thomas Malcomson[1], Alireza Azizi[2], Roya Momen[2], Tianlv Xu[2], Steven R. Kirk[*2], Martin J. Paterson[1], Samantha Jenkins[*2]

[1]*Institute of Chemical Sciences, School of Engineering and Physical Sciences, Heriot-Watt University, Edinburgh, EH14 4AS, UK*

[2]*Key Laboratory of Chemical Biology and Traditional Chinese Medicine Research and Key Laboratory of Resource National and Local Joint Engineering Laboratory for New Petro-chemical Materials and Fine Utilization of Resources, College of Chemistry and Chemical Engineering, Hunan Normal University, Changsha, Hunan 410081, China*

email: steven.kirk@cantab.net
email: samanthajsuman@gmail.com

In this investigation we considered both the scalar and 3-D vector-based measures of bonding using next generation quantum theory of atoms in molecules (QTAIM), constructed from the preferred direction of electronic charge density accumulation, to better understand the photo-chemical reaction associated with of the formation of benzvalene from benzene. The formation of benzvalene from benzene resulted in two additional C-C bonds forming compared with the benzene. The creation of the additional C-C bonds was explained in terms of an increasing the favorability of the reaction process by maximizing the bonding density. The topological instability of the benzvalene structure was determined using the scalar and vector-based measures to explain the short chemical half-life of benzvalene in terms of the competition between the formation of unstable new C-C bonding that also destabilizes nearest neighbor C-C bonds. The explosive character of benzvalene is indicated by the unusual tendency of the C-C bonds to rupture as easily as weak bonding. The topological instability of the short strong C-C bonds was explained by the existence of measures from conventional and next generation QTAIM that previously have only been observed in weak interactions such measures included twisted 3-D bonding descriptors.

Introduction

While the 1971 synthesis of benzvalene, carried out by Katz,[1] utilizing a ground state process by reacting cyclopentadiene with methyllithium and dichloromethane, this highly reactive olfin can also be produced in small quantities, alongside fulvene and Dewar benzene, through the excitation of benzene in the 245 nm range.[2] Despite benzvalene possessing a chemical half-life of only 10 days[3] before reverting back to benzene, benzvalene, along with fulvene and their associated excited state reactions are ideal to highlight the alterations in bonding structure induced through promotion of a molecule to an excited state[4–6] The ability to understand this change in bonding, see **Scheme 1**, and the insights this provides about the potential energy surface surrounding the point of vertical excitation, could be a powerful tool throughout the chemical sciences. This understanding, however, is not easily discerned, even with modern advances in theoretical chemistry.

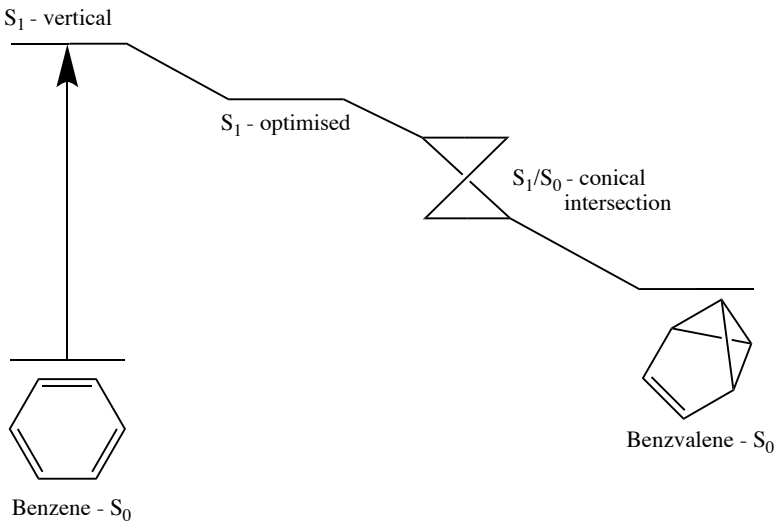

Scheme 1. The photochemical formulation of benzvalene from benzene.

It is possible, however, to gleam some information on the interpretation of excited states through the manipulation of the CASSCF wavefunction to a VB like form, gaining local orbital occupancies (charge densities) and spin-exchange coupling (P_{ij}) values, see **Table 1**.[7] For example, these electronic factors (successfully) predict that, upon optimisation in S_1, the C-C bonds extend from the 1.40 Å (2.65 a.u), found in S_0, to 1.54 Å (2.91 a.u),[7] see **Scheme 2.**

The ability to analyze and visualize the continuous evolution of the chemical bonding can be highlighted in the excited state chemistry of calicene and sesquifulvalene, derivatives of fulvene, which has been previously studied.[4–6] Despite the similarities of these compounds to fulvene, they each contain a significantly polarized central double bond, resulting in the most dominant resonance structure possessing a significantly polarized

bond. This highly polarized bond gives rise to significant charge transfer character in the lower excited state manifold[8] that will have a strong effect on the excited state chemistry of these compounds, see the C4-C5 bond in **Scheme 2**.

In this investigation therefore, we will present a new perspective of the chemical bonding of benzvalene using the 3-D, 'next-generation'[6] quantum theory of atoms in molecules (QTAIM) methodology.[9,10] Next generation QTAIM has seen an increase in applications to excited states in recent years[6] and is unique to theoretical chemistry due to being formulated as a directional 3-D vector based formulation as opposed to being comprised entirely of scalar measures that have recently been used for the prediction of stereoisomers.[11] This three-stranded 3-D interpretation of the chemical bond is more complete than minimal definition of bonding ($\underline{\mathbf{e}}_3$) the conventional QTAIM interpretation of a bond, provided by the bond-path (***r***) because it comprises all three of the $\{\underline{\mathbf{e}}_1, \underline{\mathbf{e}}_2, \underline{\mathbf{e}}_3\}$ eigenvectors. Within QTAIM the most preferred 'easy' direction $\underline{\mathbf{e}}_2$ is determined on the basis of the ease of total electronic charge density $\rho(\mathbf{r_b})$ accumulation. Conversely, the least preferred directions were found to be $\underline{\mathbf{e}}_1$ for QTAIM and $\underline{\mathbf{e}}_{2\sigma}$ for the stress tensor.[12] For the stress tensor, we have found that the $\underline{\mathbf{e}}_{1\sigma}$ eigenvector corresponds to the most preferred 'easy' direction on the basis of ease of compressibility. This finding was demonstrated using stress tensor trajectory formalism $\mathsf{T}_\sigma(s)$ in partnership with the potential energy surface to prove that the $\underline{\mathbf{e}}_{2\sigma}$ eigenvector was the least preferred direction of electronic charge density $\rho(\mathbf{r_b})$ accumulation and therefore that the $\underline{\mathbf{e}}_{1\sigma}$ eigenvector was the most preferred direction. Additional evidence for the most and least preferred directions for the stress tensor being defined by the $\underline{\mathbf{e}}_{1\sigma}$ and $\underline{\mathbf{e}}_{2\sigma}$ eigenvector was provided by the fact that the values for $\mathsf{H}_\sigma^* > \mathsf{H}_\sigma$ and $\mathsf{H}_{\sigma H}^* > \mathsf{H}_{\sigma H}$ consistent with previous findings from QTAIM that the preferred path has the longer associated eigenvector following path length.

Previously, some of the current authors demonstrated that the stress tensor can be used within the QTAIM partitioning scheme by using next generation QTAIM.[12] This analysis was undertaken using an adapted version of the recently introduced 3-D *vector-based* interpretation of the chemical bond $\mathsf{B} = \{\boldsymbol{p},\boldsymbol{q},\boldsymbol{r}\}$ of the form $\mathsf{B}_\sigma = \{\boldsymbol{p}_\sigma,\boldsymbol{q}_\sigma,\boldsymbol{r}\}$ to follow changes in the directional properties of the stress tensor that is robust to electronic excitations. We demonstrated that the construction of $\mathsf{B}_\sigma = \{\boldsymbol{p}_\sigma,\boldsymbol{q}_\sigma,\boldsymbol{r}\}$ that used $\varepsilon_\sigma \leq 0$ the most closely approximated the $\mathsf{B} = \{\boldsymbol{p},\boldsymbol{q},\boldsymbol{r}\}$. This is because the 'easy' direction for the stress tensor is determined by the most compressible $\lambda_{1\sigma}$ i.e. associated with the longer axis of the ellipse, whereas for QTAIM the 'easy' direction, (longer axis of the ellipse) is associated with the λ_2 eigenvalue.

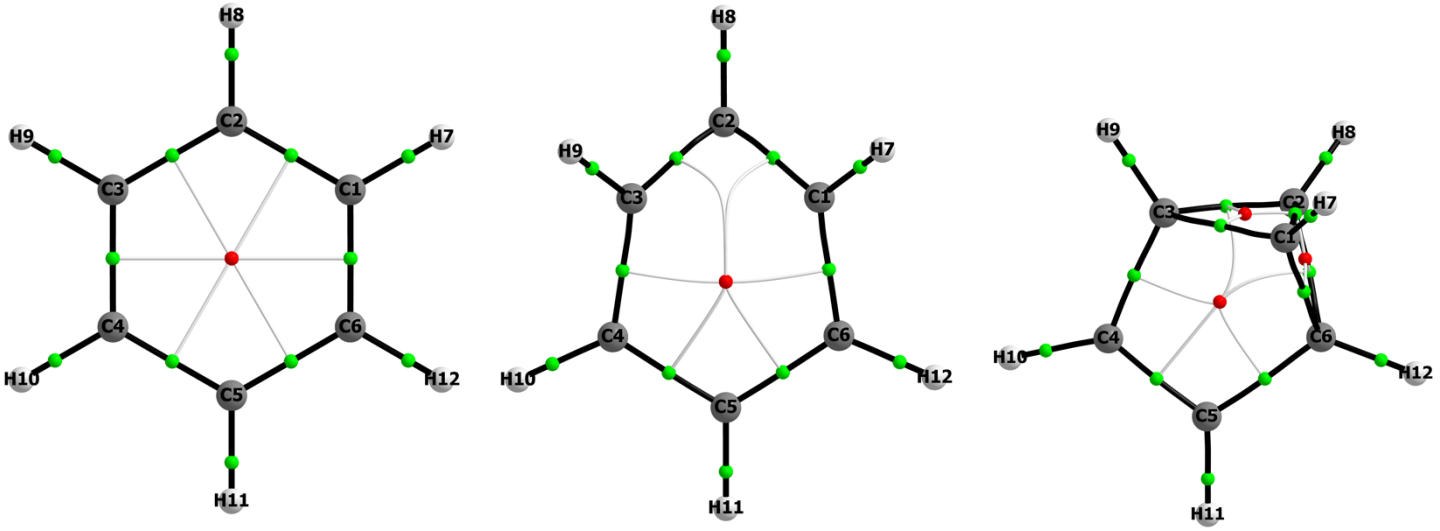

Scheme 2. The benzene S_0, benzene S_1vert and benzene S_1opt (left), benzvalene S_0/S_1 ContInt (middle) and benzvalene S_0 (right) molecular graphs, the bond-path (***r***) is indicated by the black lines with the undecorated green and red spheres representing the bond critical point (*BCP*s) and ring critical points (*RCP*s), respectively, with the white lines indicating the *RCP-BCP* paths.

Recently,[5] we provided a 3-D understanding of the bonding provided by using Lewis structures for the ground state S_0 and first excited state S_1 of fulvene. We discovered that the corresponding bond-path framework set $B_{0,1}$ = $\{(\boldsymbol{p}_0,\boldsymbol{p}_1),(\boldsymbol{q}_0,\boldsymbol{q}_1),(\boldsymbol{r}_0,\boldsymbol{r}_1)\}$, was better approximated by the stress tensor formulation $B_{\sigma 0,1}$ = $\{(\boldsymbol{p}_{\sigma 0},\boldsymbol{p}_{\sigma 1}),(\boldsymbol{q}_{\sigma 0},\boldsymbol{q}_{\sigma 1}),(\boldsymbol{r}_0,\boldsymbol{r}_1)\}$ than $B_{\sigma H0,1}$ = $\{(\boldsymbol{p}_{\sigma H0},\boldsymbol{p}_{\sigma H1}),(\boldsymbol{q}_{\sigma H0},\boldsymbol{q}_{\sigma H1}),(\boldsymbol{r}_0,\boldsymbol{r}_1)\}$. The stress tensor $B_{\sigma H0,1}$, with the associated eigenvector path lengths is provided for the readers interest in the **Supplementary Materials S4**.
In this investigation therefore, we use will next Generation QTAIM to follow changes of the chemical bonding character in 3-D for the photochemical synthesis of benzvalene from benzene.

2. Theory and Methods

2.1 The QTAIM and stress tensor BCP properties; the ellipticity ε and the stress ellipticities $\varepsilon_{\sigma H}$ and ε_{σ}

Within the QTAIM framework other representations of the chemical bond include bond-bundles in open systems, where molecules are partitioned where bounded regions of space containing non-bonding or lone-pair electrons are created that lead to bond orders consistent with expectation from theories of directed valence.[13,14] In this investigation QTAIM[9] is used to identify critical points in the total electronic charge density distribution $\rho(\mathbf{r})$ by analyzing the gradient vector field $\nabla\rho(\mathbf{r})$. These critical points can further be divided into four types of topologically stable critical points according to the set of ordered eigenvalues $\lambda_1 < \lambda_2 < \lambda_3$, with corresponding

eigenvectors $\underline{\mathbf{e}}_1$, $\underline{\mathbf{e}}_2$, $\underline{\mathbf{e}}_3$ of the Hessian matrix. The Hessian of the total electronic charge density $\rho(\mathbf{r})$ is defined as the matrix of partial second derivatives with respect to the spatial coordinates. We use the notation (R, ω) where R is the rank of the Hessian matrix, the number of distinct non-zero eigenvalues and ω is the signature (the algebraic sum of the signs of the eigenvalues) to label the critical points; the (3, -3) [nuclear critical point (*NCP*), a local maximum corresponding to a nuclear location], (3, -1) and (3, 1) [saddle points, bond critical points (*BCP*), ring critical points (*RCP*)] and (3, 3) [the cage critical points (*CCP*)]. An atomic interaction line[15] is referred to as a *bond-path* in the limit that the forces on the nuclei become vanishingly small, although not necessarily a chemical bond.[16] The completed set of critical points together with the bond-paths of a molecule or cluster is referred to as the molecular graph.

The eigenvector $\underline{\mathbf{e}}_3$ indicates the direction of the bond-path at the *BCP*. The most and least preferred directions of electron accumulation are $\underline{\mathbf{e}}_2$ and $\underline{\mathbf{e}}_1$, respectively.[17–19] The ellipticity ε provides a measure of the aromatic character where a double bond is indicated for shared-shell BCPs with approximate values of the ellipticity ε ≈ 0.25 or more and a single bond for ellipticity ε ≈ 0.10 or less. The ellipticity ε also determines the relative accumulation of $\rho(\mathbf{r_b})$ in the two directions perpendicular to the bond-path at a *BCP*, defined as $\varepsilon = |\lambda_1|/|\lambda_2| - 1$ where λ_1 and λ_2 are negative eigenvalues of the corresponding eigenvectors $\underline{\mathbf{e}}_1$ and $\underline{\mathbf{e}}_2$ respectively. Recently, for the 11-cis retinal subjected to a torsion ±θ, we have also demonstrated that the $\underline{\mathbf{e}}_2$ eigenvector of the torsional *BCP* corresponded to the preferred +θ direction of rotation as defined by the PES profile.[20] Previously, we defined a bond-path *BCP* stiffness, $\mathsf{S} = |\lambda_2|/\lambda_3$, as a measure of rigidity of the bond-path.[21] The total local energy density $H(\mathbf{r}_b)$[4,22] is defined as:

$$H(\mathbf{r}_b) = G(\mathbf{r}_b) + V(\mathbf{r}_b), \qquad \textbf{(1)}$$

where $G(\mathbf{r}_b)$ and $V(\mathbf{r}_b)$ in equation (**1**) are the local kinetic and potential energy densities at a *BCP*.

The quantum stress tensor, $\sigma(\mathbf{r})$, is directly related to the Ehrenfest force by the virial theorem and so provides a physical explanation of the low-frequency normal modes that accompany structural rearrangements.[17,23,24] There are several versions, but in this investigation we will use Bader's definition.[25,26] The stress tensor eigenvalue associated with the bond-path; $\lambda_{3\sigma}$, the tensile eigenvalue, where values of $\lambda_{3\sigma} < 1$ have been associated with an incommensurate gas to solid phase transition in biphenyl[21] and transition-type behavior in molecular motors.[27] Therefore, in this investigation we use more negative values of $\lambda_{3\sigma}$ to quantify a greater degree of topological instability that indicates a greater tendency for structural transformation and therefore reactivity.

In this investigation we will use the two ellipticities defined for use with for the stress tensor:

$$\varepsilon_{\sigma H} = |\lambda_{1\sigma}|/|\lambda_{2\sigma}| - 1, \quad \varepsilon_{\sigma} = |\lambda_{2\sigma}|/|\lambda_{1\sigma}| - 1 \qquad \textbf{(2)}$$

Where the subscript '$_H$' of $\varepsilon_{\sigma H}$ in equation **(2)** refers to the use of the most/least negative eigenvalues for the eigenvalues of numerator/denominator as the QTAIM ellipticity ε, consequently the stress tensor ellipticity $\varepsilon_{\sigma H} \geq 0$ and the ellipticity $\varepsilon \geq 0$ without exception, due to the eigenvalues being ordered $\lambda_{1\sigma} < \lambda_{2\sigma} < \lambda_{3\sigma}$ and $\lambda_1 < \lambda_2 < \lambda_3$. Conversely, equation **(2)** that defines ε_σ uses the least/most negative eigenvalues for the eigenvalues of numerator/denominator and due to the eigenvalues being ordered $\lambda_{1\sigma} < \lambda_{2\sigma} < \lambda_{3\sigma}$ then $\varepsilon_\sigma \leq 0$ without exception.
Where for the stress tensor the 'easy' direction ($\underline{\mathbf{e}}_{1\sigma}$) is determined by the most compressible eigenvalue $\lambda_{1\sigma}$ i.e. associated with the longer axis of the ellipse associated with ellipticity. Conversely, for QTAIM the 'easy' direction ($\underline{\mathbf{e}}_2$) is associated with the longer axis (λ_2) of the ellipse. This is because for QTAIM there is an ellipse shaped distribution in $\rho(\mathbf{r_b})$ for values of $\varepsilon > 0$, perpendicular to the bond-path with long (associated with the 'easy' direction $\underline{\mathbf{e}}_2$) and short (associated with the 'hard' direction $\underline{\mathbf{e}}_1$) axes defined by the λ_2 and λ_1 eigenvalues respectively.

2.2 The QTAIM, $B = \{\boldsymbol{p},\boldsymbol{q},\boldsymbol{r}\}$ and stress tensor bond-path framework set $B_{\sigma H} = \{\boldsymbol{p}_{\sigma H},\boldsymbol{q}_{\sigma H},\boldsymbol{r}\}$ and $B_\sigma = \{\boldsymbol{p}_\sigma,\boldsymbol{q}_\sigma,\boldsymbol{r}\}$

The bond-path length (BPL) is defined as the length of the path traced out by the $\underline{\mathbf{e}}_3$ eigenvector of the Hessian of the total charge density $\rho(\mathbf{r})$, passing through the *BCP*, along which $\rho(\mathbf{r})$ is locally maximal with respect to any neighboring paths. The bond-path curvature separating two bonded nuclei is defined as the dimensionless ratio:

$$(\text{BPL} - \text{GBL})/\text{GBL}, \qquad \textbf{(3)}$$

Where the BPL is the associated bond-path length and the geometric bond length GBL is the inter-nuclear separation. The BPL very often exceeds the GBL for weak or strained bonds in unusual bonding environments.[28] For 3-D bond-paths, there are two radii curvature specified by minor and major radii and defined by the directions of $\underline{\mathbf{e}}_2$ and $\underline{\mathbf{e}}_1$ respectively.[29]
Two paths (***q*** *and* ***q***') are defined as being associated with the $\underline{\mathbf{e}}_2$ eigenvector since $\underline{\mathbf{e}}_2 \equiv -\underline{\mathbf{e}}_2$ lies in the same plane for the same point on the bond-path (***r***); correspondingly there are two paths associated with the $\underline{\mathbf{e}}_1$ (***p*** and ***p***'), see equation **(4)**. We will present the {***q***,***q'***} path-packets and the {***p***,***p'***} path-packets to make viewing of the aromatic character more convenient. This is because by definition the {***q***,***q'***} path-packets are always orthogonal to the {***p***,***p'***} path-packets but the aromatic character will be not apparent when the {***q***,***q'***} path-packets are edge on to the viewing plane. The form of the constituent {***q***,***q'***},{***p***,***p'***} path-packets can be used to provide a 3-D interpretation of bonding as a mixture of the following concepts: double bond, single bond, covalent, ionic or diradical. Note that, double and single bonds for shared-shell *BCP*s correspond to values of the *BCP* ellipticity

$\varepsilon > 0.25$ and $\varepsilon < 0.25$ respectively, also the $\{\boldsymbol{q},\boldsymbol{q}'\}$ and $\{\boldsymbol{p},\boldsymbol{p}'\}$ path-packets have no enclosed area for values of the ellipticity $\varepsilon = 0$. An ionic interaction is characterized by a dominant peak in the $\{\boldsymbol{q},\boldsymbol{q}'\}$ path-packets closer to one atom that the other.[30] Recently, we examined the $\{\boldsymbol{q},\boldsymbol{q}'\},\{\boldsymbol{p},\boldsymbol{p}'\}$ path-packets with the stress tensor $\{\boldsymbol{q}_\sigma,\boldsymbol{q}'_\sigma\}$, $\{\boldsymbol{p}_\sigma,\boldsymbol{p}'_\sigma\}$ path-packets for the torsion of ethane.[12] Note that the stress tensor $\{\boldsymbol{q}_\sigma,\boldsymbol{q}'_\sigma\}$ and $\{\boldsymbol{p}_\sigma,\boldsymbol{p}'_\sigma\}$ path-packets are constructed using the stress tensor ellipticity $\varepsilon_\sigma = |\lambda_{2\sigma}|/|\lambda_{1\sigma}| - 1$:

$$\boldsymbol{p}_i = \boldsymbol{r}_i + \varepsilon_i \underline{\mathbf{e}}_{1,i}, \;\; \boldsymbol{q}_i = \boldsymbol{r}_i + \varepsilon_i \underline{\mathbf{e}}_{2,i} \qquad \textbf{(4)}$$

In the limit of vanishing ellipticity $\varepsilon = 0$, *for all* steps i along the bond-path then $\mathsf{H} = \mathrm{BPL}$, the lengths of the $\boldsymbol{p}$- and $\boldsymbol{q}$-paths are defined as the *eigenvector-following paths* H^* or H**:**

$$\mathsf{H}^* = \sum^{n-1}_{i=1} |\boldsymbol{p}_{i+1} - \boldsymbol{p}_i|, \;\; \mathsf{H} = \sum^{n-1}_{i=1} |\boldsymbol{q}_{i+1} - \boldsymbol{q}_i| \qquad \textbf{(5)}$$

The term $\{\boldsymbol{q},\boldsymbol{q}'\}$ path-packet is used to refer to the orbital-like packet shapes that the pair of $\boldsymbol{q}$- and $\boldsymbol{q}$'-paths form along the bond-path. The 3-D path-packets present a visualization of the direction and degree of bond-path linearity or torsion. The shape and location of the $\{\boldsymbol{q},\boldsymbol{q}'\}$ path-packet relative to the *BCP*, e.g. a long planar $\{\boldsymbol{q},\boldsymbol{q}'\}$ path-packet that envelopes the *BCP*, indicates the greater ease of sliding motion of the *BCP*, bond-path and associated *NCP*s than for a $\{\boldsymbol{q},\boldsymbol{q}'\}$-path packet that is twisted or localized to the *BCP*. Extremely long $\{\boldsymbol{q},\boldsymbol{q}'\}$ path-packets predict imminent *BCP* rupture due to the coalescence and annihilation of a *BCP* and a neighboring *RCP*. The complete set of $\{\boldsymbol{q},\boldsymbol{q}'\},\{\boldsymbol{p},\boldsymbol{p}'\}$ and $\boldsymbol{r}$ constitute the bond-path-framework set $\mathsf{B} = \{\boldsymbol{p},\boldsymbol{q},\boldsymbol{r}\}$ and for the stress tensor $\mathsf{B}_\sigma = \{\boldsymbol{p}_\sigma,\boldsymbol{q}_\sigma,\boldsymbol{r}\}$, the **Supplementary Materials S1** for further discussion including the choice of the ellipticity ε as the scaling factor.

In addition, we will check the comparison with the stress tensor for excited states using the bond-path framework set $\mathsf{B}_{\sigma\mathrm{H}} = \{\boldsymbol{p}_{\sigma\mathrm{H}},\boldsymbol{q}_{\sigma\mathrm{H}},\boldsymbol{r}\}$ lengths $\mathsf{H}_{\sigma\mathrm{H}}$ and $\mathsf{H}_{\sigma\mathrm{H}}^*$ and also $\mathsf{B}_\sigma = \{\boldsymbol{p}_\sigma,\boldsymbol{q}_\sigma,\boldsymbol{r}\}$ with corresponding lengths H_σ and H_σ^* using the definitions of the ellipticities $\varepsilon_{\sigma\mathrm{H}}$ and ε_σ defined by equation **(5)** and equation **2(a-b)** respectively in the **Supplementary Materials S1**. In this investigation we will examine the relative orientation of the $\{\boldsymbol{q},\boldsymbol{q}'\}$, $\{\boldsymbol{p},\boldsymbol{p}'\}$ path-packets states as well as the stress tensor $\{\boldsymbol{q}_\sigma,\boldsymbol{q}'_\sigma\}$, $\{\boldsymbol{p}_\sigma,\boldsymbol{p}'_\sigma\}$ in addition to the $\{\boldsymbol{q}_\sigma,\boldsymbol{q}'_\sigma\}$, $\{\boldsymbol{p}_\sigma,\boldsymbol{p}'_\sigma\}$ path-packets, see equation **3(a-b**), to the aromatic plane for the planar and twisted conformations in all cases we consider both in the ground S_0 and first excited S_1 electronic states. When the BPL = GBL, then (BPL - GBL)/GBL = 0 from equation **(3)** and therefore a linear bond-path then the lengths of the $\{\boldsymbol{q},\boldsymbol{q}'\},\{\boldsymbol{p},\boldsymbol{p}'\}$ path-packets specified as (H,H') and $(\mathsf{H}^*,\mathsf{H}^{*\prime})$ respectively will all be the same length i.e. $\mathsf{H} = \mathsf{H}' = \mathsf{H}^* = \mathsf{H}^{*\prime}$. For a non-linear bond-path (BPL - GBL)/GBL > 0 and BPL > GBL then we define by convention that $\mathsf{H} > \mathsf{H}'$ and $\mathsf{H}^* < \mathsf{H}^{*\prime}$.

3. Computational Details

All structures where optimised using a CASSCF wavefunction built around a (6,6) active space, and the 6-311G(d,p) basis via Gaussian16 (revision A3). CASSCF occupancies were obtained via localisation of the π-orbitals in the active space to p_π atom centered orbitals via the Boys localisation procedure.[31] The two-particle spin-exchange density matrix (P) was then constructed from these localised orbitals to generate a VB analysis of the relevant states. The spin-exchange density is a two-particle density matrix, obtained as the expectation value of the following operator (assuming a configuration interaction type wavefunction),

$$P_{ij} = \left\langle \frac{1}{2}(\hat{E}_{ij}^{\alpha\alpha}\hat{E}_{ji}^{\beta\beta} + \hat{E}_{ij}^{\beta\beta}\hat{E}_{ji}^{\alpha\alpha} + \hat{E}_{ij}^{\alpha\alpha}\hat{E}_{ji}^{\alpha\alpha} - \hat{E}_{ii}^{\alpha\alpha} + \hat{E}_{ij}^{\beta\beta}\hat{E}_{ji}^{\beta\beta} - \hat{E}_{ii}^{\beta\beta}) \right\rangle \quad \textbf{(6)}$$

where $\hat{E}_{ij}^{\sigma\sigma} = a_{i\sigma}^{\dagger}a_{j\sigma}$ are the generators of the unitary group U(n), and $\sigma = \alpha$ or β.These matrix elements (P_{ij}) have a simple interpretation that helps one to understand the spin coupling.[7] For a single configuration perfectly paired valence bond (VB) wave function the P_{ij} have values of +1 for a singlet-coupled pair, -1 for a triplet coupled pair and -1/2 when the pair is uncoupled. Configuration interaction will cause the actual computed values to differ from these idealized values and it is common to take a positive P_{ij} as singlet coupled and a negative P_{ij} as uncoupled.[32,33] The QTAIM and stress tensor analysis was performed with the AIMAll[34] suite on each wave function obtained in the previous step. The calculated paths comprising the $B_{0,1}$, $B_{\sigma 0,1}$ and $B_{\sigma H 0,1}$ were visualized using the Python 3 visualization toolkit Mayavi.[35]

4. Results and discussions

4.1 P_{ij} analysis of S_1/S_0 conical intersection:

As mentioned previously, the CASSCF P_{ij} analysis of the benzene $S_0 \rightarrow S_1$ transition shows a reduction in the coupling values of all bonds from 0.337 to 0.252, corresponding to weakening of the double bond character inherent in the S_0 electronic structure; this change acts to explain the observed bond lengthening in the S_1 structure. At the point of the conical intersection P_{ij} values suggest that the electronic structure on the S_1 surface resembles what would be expected from cyclohexatriene, with an alternating pattern of strongly singlet coupled and uncoupled bonds, while no coupling is seen across the ring (**Table 1**); whereas, on the S_0 surface we observe the emergence of the weakly coupled, three centered electronic structure of prefulvene, corresponding to a -CH_3- kink in the carbon framework.[36] Looking at the coupling values that would drive bond formation in the benzvalene final product, see **Table 1**, there is a symmetrical coupling between C2 and both C4 and C6 characterising the out of plane movement of the C2 centre in the positive direction of the S_1 transition vector;

however, an asymmetrical coupling is observed from C_1 to C_3 and C_5 (0.555 and 0.014, respectively), suggesting a preferential formation of the C_1-C_3 bond, leading to the benzvalene structure shown in **Scheme 2.**

Table 1. Selected P_{ij} coupling values for each member of the degenerate pair of states at the S_1/S_0 conical intersection geometry**;** see also **Scheme 1** and **Scheme 2**

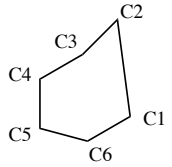	S_0	S_1
1-2	0.046	-0.320
1-3	0.555	0.003
1-5	0.014	-0.022
1-6	0.083	0.216
2-3	0.039	0.316
2-4	0.476	-0.089
2-6	0.474	0.094
3-4	0.087	-0.218
4-5	0.395	0.171
5-6	0.398	-0.170

4.2 A QTAIM bond-path framework set analysis of benzene and benzvalene

The photo-chemical reaction of the formation of benzvalene from benzene process is as follows: the vertical excitation of benzene in the ground state (S_0) to the first excited state of benzene (S_1vert) by a vertical excitation, followed by the optimized excited state structure (S_1opt) before reaching the conical intersection with the ground state (S_0/S_1ConInt) and finally relaxing down to the ground state of benzvalene (S_0), see **Scheme 1** and **Scheme 2**.

Examination of the *BCP* properties provides a summarized view of the bonding changes during the photo-reaction, see **Table 2**. For the vertical excitation; benzene $S_0 \rightarrow S_1$vert the ellipticity $\varepsilon = 0.23$, that indicates significant double bond character, as expected in the benzene C-C bond, decreases to $\varepsilon = 0.18$, indicating a substantially higher degree of single bond character, providing agreement with both previously investigated P_{ij} values[7] and those presented here. After the vertical excitation, the value stiffness S increases instead of

decreasing, as would be expected for a decrease in double bond character. The remaining measures; charge density $\rho(\mathbf{r}_b)$, Laplacian $\nabla^2\rho(\mathbf{r}_b)$, total local energy density $H(\mathbf{r}_b)$ and stress tensor eigenvalue $\lambda_{3\sigma}$ do not change significantly.

The $\rho(\mathbf{r}_b)$, $\nabla^2\rho(\mathbf{r}_b)$, $|H(\mathbf{r}_b)|$ and S all decrease for benzene S_1vert → benzene S_1opt due to the lengthening of the C-C bonds, however, the ellipticity ε and $\lambda_{3\sigma}$ do not change significantly as symmetry has not been broken. The symmetry breaking step next occurs for the benzene S_1 opt → benzvalene S_0/S_1ConInt, all of the *BCP* values significantly spread out except for the *BCP* instability value $\lambda_{3\sigma}$ that is associated with transitional behavior, see the theory section 2.1. In particular, the C4-C5 *BCP* and the C5-C6 *BCP* emerge with similar, significantly stronger ellipticity ε values, i.e. an increase in double bond character that possess greater stiffness S than the remaining *BCP*s comprising the benzvalene S_0/S_1ConInt molecular graph. The final step; benzvalene S_0/S_1ConInt → benzvalene S_0 the C4-C5 *BCP* possess double bond character with the highest $H(\mathbf{r}_b)$ and S values whilst also being the most topologically unstable, i.e. tendency for the *BCP* to rupture resulting in the breakdown of the molecular framework, on the basis of the least positive $\lambda_{3\sigma}$ value. The C3-C4 *BCP* and C5-C6 *BCP*, that neighbor the C4-C5 *BCP*, possess single bond character on the basis of low values of the ellipticity ε < 0.1 that are the most stable, having the highest values of stiffness S, leading to the conflicting behavior of the chemical character, this issue is addressed in the next section in terms of the $\{\boldsymbol{q},\boldsymbol{q'}\}$ path-packets.

The bonding increases on the final step benzvalene S_0/S_1ConInt → benzvalene S_0 with the formation of the C1-C3 *BCP* and the C2-C6 *BCP* and consequently two new *RCP*s are formed.

Table 2. The QTAIM and stress tensor *BCP* properties in a.u.; the total charge density $\rho(\mathbf{r}_b)$, Laplacian $\nabla^2\rho(\mathbf{r}_b)$, ellipticity ε, total local energy density $H(\mathbf{r}_b)$, stiffness $\mathsf{S} = |\lambda_2|/\lambda_3$ and the stress tensor tensile eigenvalue $\lambda_{3\sigma}$ of the benzene S_0, benzene S_1vert, benzene S_1opt, benzvalene S_0/S_1ConInt and benzvalene S_0 molecular graphs, see **Scheme 1** for a sketch of the photo-reaction and **Scheme 2** for the atomic numbering.

	benzene S_0						benzene S_1vert					
BCP	$\rho(\mathbf{r}_b)$	$\nabla^2\rho(\mathbf{r}_b)$	ε	$H(\mathbf{r}_b)$	S	$\lambda_{3\sigma}$	$\rho(\mathbf{r}_b)$	$\nabla^2\rho(\mathbf{r}_b)$	ε	$H(\mathbf{r}_b)$	S	$\lambda_{3\sigma}$
C1-C2	0.320	-0.975	0.227	-0.335	2.059	0.061	0.321	-1.000	0.183	-0.337	2.160	0.060

	benzene S_1opt					
	$\rho(\mathbf{r}_b)$	$\nabla^2\rho(\mathbf{r}_b)$	ε	$H(\mathbf{r}_b)$	S	$\lambda_{3\sigma}$
	0.298	-0.864	0.184	-0.293	1.843	0.064

	benzvalene S_0/S_1ConInt						benzvalene S_0					
	$\rho(\mathbf{r}_b)$	$\nabla^2\rho(\mathbf{r}_b)$	ε	$H(\mathbf{r}_b)$	S	$\lambda_{3\sigma}$	$\rho(\mathbf{r}_b)$	$\nabla^2\rho(\mathbf{r}_b)$	ε	$H(\mathbf{r}_b)$	S	$\lambda_{3\sigma}$
C1-C2	0.284	-0.772	0.164	-0.275	1.692	0.062	0.251	-0.396	0.217	-0.225	1.004	0.048
C2-C3	0.284	-0.773	0.165	-0.275	1.691	0.062	0.251	-0.542	0.366	-0.220	1.206	0.056
C3-C4	0.281	-0.753	0.228	-0.264	1.628	0.063	0.262	-0.694	0.084	-0.230	1.572	0.063
C4-C5	0.319	-0.957	0.263	-0.335	2.011	0.059	0.349	-1.086	0.399	-0.402	2.460	0.046
C5-C6	0.319	-0.959	0.259	-0.335	2.017	0.059	0.262	-0.691	0.083	-0.229	1.566	0.063
C6-C1	0.281	-0.751	0.233	-0.264	1.621	0.063	0.246	-0.503	0.469	-0.213	1.110	0.054
C1-C3	----	----	----	----	----	----	0.224	-0.357	0.587	-0.178	0.814	0.047
C2-C6	----	----	----	----	----	----	0.246	-0.503	0.463	-0.213	1.109	0.054

To explain these findings and provide a less localized descriptor than the *BCP* we now consider the bond-path framework set $\mathsf{B}_{0,1} = \{(\boldsymbol{p}_0,\boldsymbol{p}_1), (\boldsymbol{q}_0,\boldsymbol{q}_1), (\boldsymbol{r}_0,\boldsymbol{r}_1)\}$, see **Scheme 2**, **Figure 1** and **Table 3**. We present the $\{\boldsymbol{q},\boldsymbol{q'}\}$ (magenta lines) and $\{\boldsymbol{p},\boldsymbol{p'}\}$ path-packets (blue lines) side-by-side since the $\{\boldsymbol{p},\boldsymbol{p'}\}$ show the approximate in plane and therefore hidden view of the $\{\boldsymbol{q},\boldsymbol{q'}\}$ path-packets, for additional viewing angles see the **Supplementary Materials S2**.

Examination of the vertical excitation, benzene $S_0 \rightarrow S_1$vert, the symmetrical $\{\boldsymbol{q},\boldsymbol{q'}\}$ path-packets that occur around each of the C-C *BCPs* indicates the presence of significant double bond character, see **Table 1**. A slightly greater than 1% decrease in lengths of the $\{\boldsymbol{q},\boldsymbol{q'}\}$ path-packets, given by the lengths (H,H′), occurs for this vertical excitation, see **Table 3**. Where an increase/decrease in (H,H′) value is associated with a increase/decrease in the double bond character for a shared-shell *BCP* and an increased/decreased tendency to rupture for a closed-shell *BCP*. For the next step, benzene S_1vert → S_1opt the inter-nuclear separation (GBL) increases as expected, yields an identical geometry and bond-path length from conventional QTAIM, indicated by GBL and BPL respectively.

The $\{\boldsymbol{q},\boldsymbol{q'}\}$ path-packets of the benzvalene C1-C3 *BCP*, C2-C3 *BCP*, C1-C6 *BCP* and C2-C6 *BCP* are large and *twisted* in the plane that contains the *RCP-BCP* separation, see the left panel of **Figure 1(e)** and the *RCP-BCP* lines in **Scheme 2**. This is not characteristic of the $\{\boldsymbol{q},\boldsymbol{q'}\}$ path-packets of a shared-shell *BCP*, but would be

expected for a closed-shell *BCP*. More expected is the $\{\boldsymbol{q},\boldsymbol{q'}\}$ path-packets associated with benzene C-C *BCP*s that are oriented perpendicular to the *RCP-BCP* separation. Consistency is found with the stress tensor bond-path framework set $\mathsf{B}_{\sigma 0,1} = \{(\boldsymbol{p}_{\sigma 0},\boldsymbol{p}_{\sigma 1}),(\boldsymbol{q}_{\sigma 0},\boldsymbol{q}_{\sigma 1}),(\boldsymbol{r}_0,\boldsymbol{r}_1)\}$, see **Figure 2** and the **Supplementary Materials S3**.

Table 3. The eigenvector following path lengths (H,H′) and (H^*,$H^{*\prime}$) of the associated with the $\{\boldsymbol{q},\boldsymbol{q'}\}$ and $\{\boldsymbol{p},\boldsymbol{p'}\}$ path-packets respectively, along with the bond-path lengths (BPL) and geometric bond lengths (GBL) in Ångstrom, see the caption of **Scheme 1**, **Scheme 2**, **Figure 1** and **Figure 2** for further details.

benzene S_0

BCP	(H,H′)	(H^*,$H^{*\prime}$)	(BPL, GBL)
C1-C2	(1.458, 1.458)	(1.458, 1.458)	(1.396, 1.396)

benzene S_1vert

(H,H′)	(H^*,$H^{*\prime}$)	(BPL,GBL)
(1.441, 1.441)	(1.441, 1.441)	(1.396, 1.396)

benzene S_1opt

(H,H′)	(H^*,$H^{*\prime}$)	(BPL, GBL)
(1.482, 1.482)	(1.482, 1.482)	(1.435, 1.435)

benzvalene S_0/S_1ConInt

	(H,H′)	(H^*,$H^{*\prime}$)	(BPL, GBL)
C1-C2	(1.506, 1.485)	(1.491, 1.499)	(1.462, 1.454)
C2-C3	(1.505, 1.484)	(1.491, 1.498)	(1.462, 1.454)
C3-C4	(1.545, 1.541)	(1.542, 1.544)	(1.467, 1.466)
C4-C5	(1.511, 1.499)	(1.501, 1.510)	(1.395, 1.395)
C5-C6	(1.508, 1.496)	(1.498, 1.507)	(1.395, 1.395)
C6-C1	(1.548, 1.544)	(1.545, 1.547)	(1.467, 1.466)
C1-C3	(----, ----)	(----, ----)	(----, ----)
C2-C6	(----, ----)	(----, ----)	(----, ----)

benzvalene S_0

(H,H′)	(H^*,$H^{*\prime}$)	(BPL, GBL)
(1.545, 1.544)	(1.535, 1.556)	(1.482, 1.462)
(1.767, 1.690)	(1.704, 1.747)	(1.514, 1.503)
(1.537, 1.536)	(1.534, 1.539)	(1.513, 1.512)
(1.539, 1.539)	(1.523, 1.555)	(1.343, 1.342)
(1.538, 1.537)	(1.535, 1.540)	(1.515, 1.514)
(1.878, 1.795)	(1.804, 1.859)	(1.520, 1.510)
(2.014, 1.939)	(1.931, 2.005)	(1.562, 1.552)
(1.846, 1.767)	(1.775, 1.829)	(1.520, 1.510)

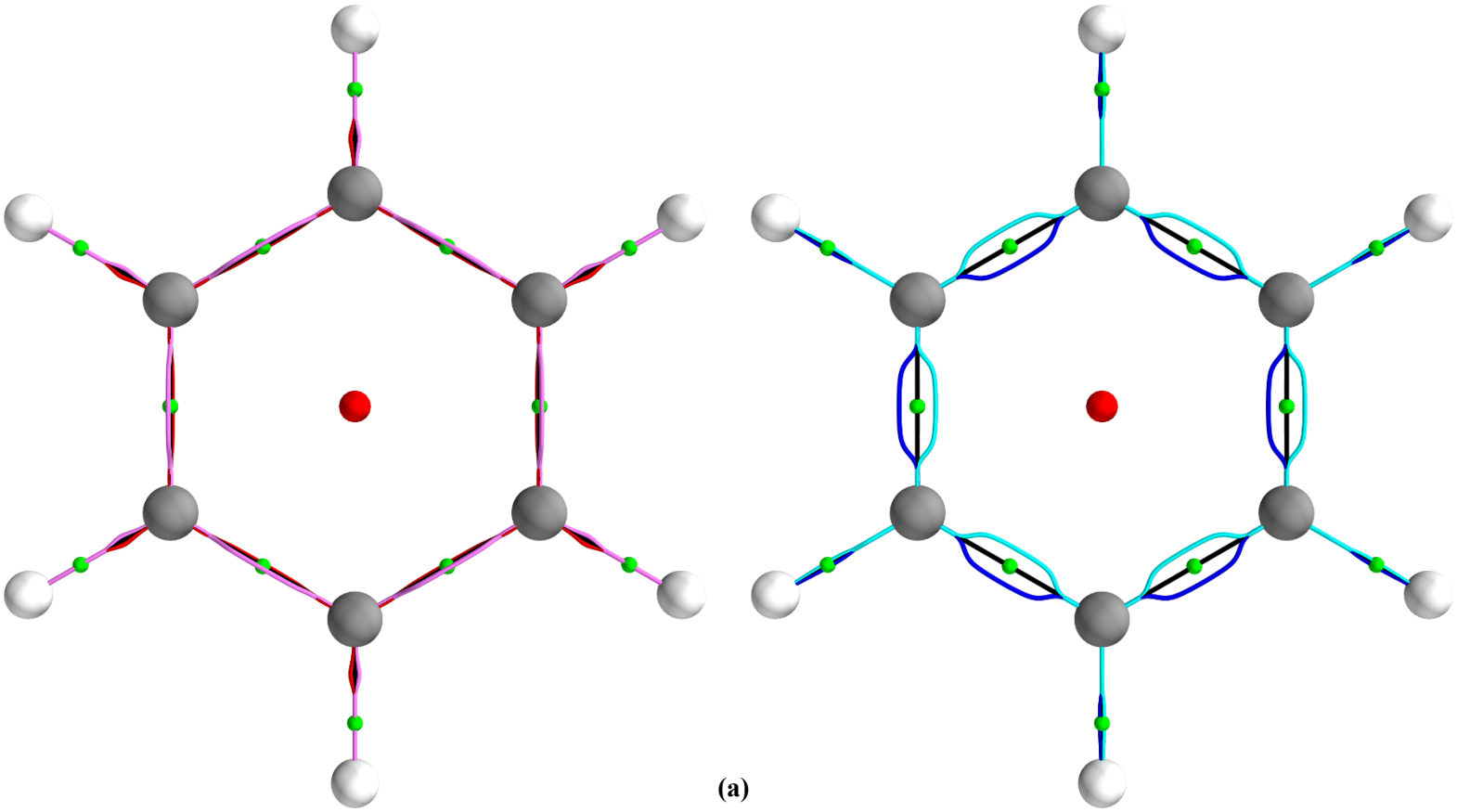

(a)

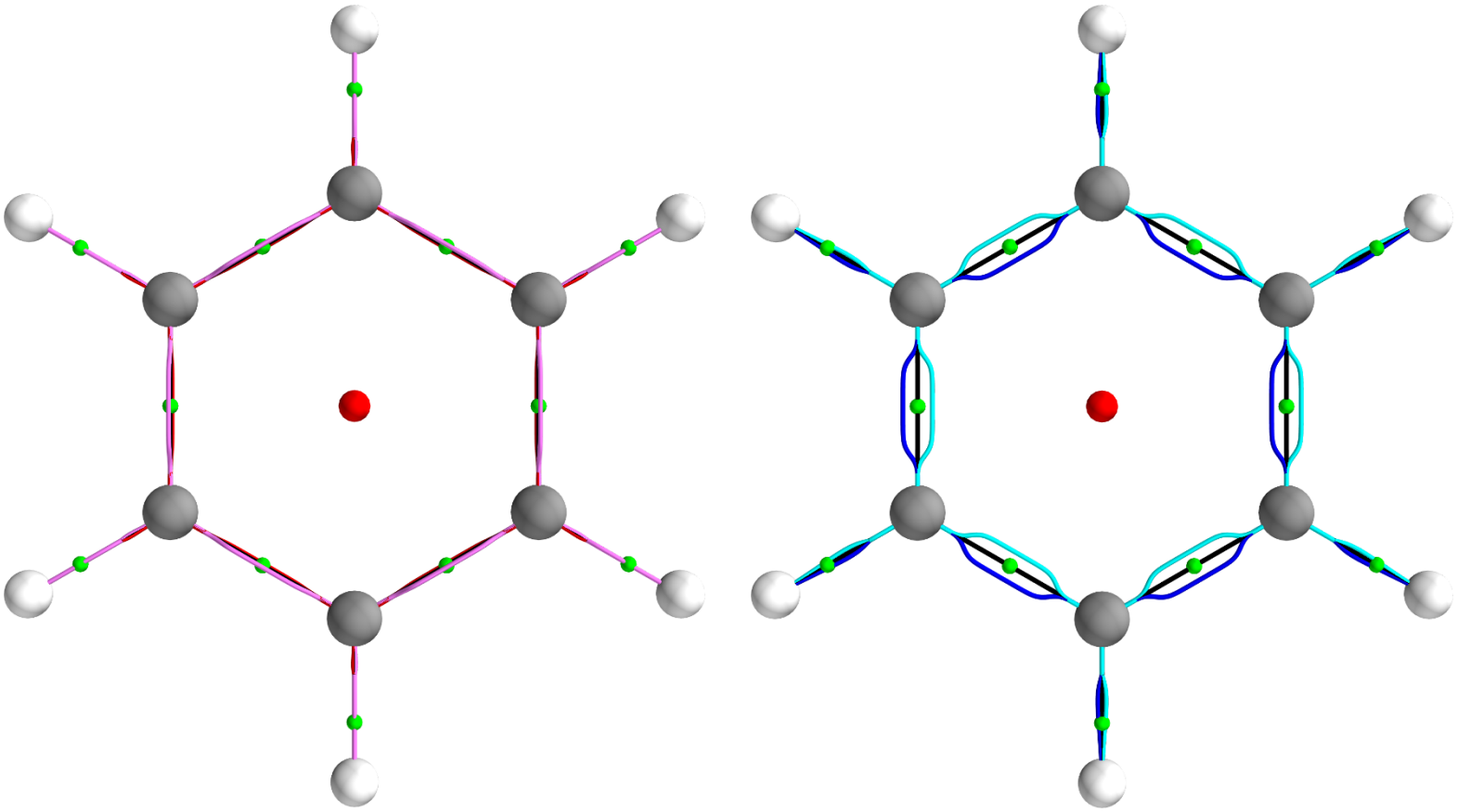

(b)

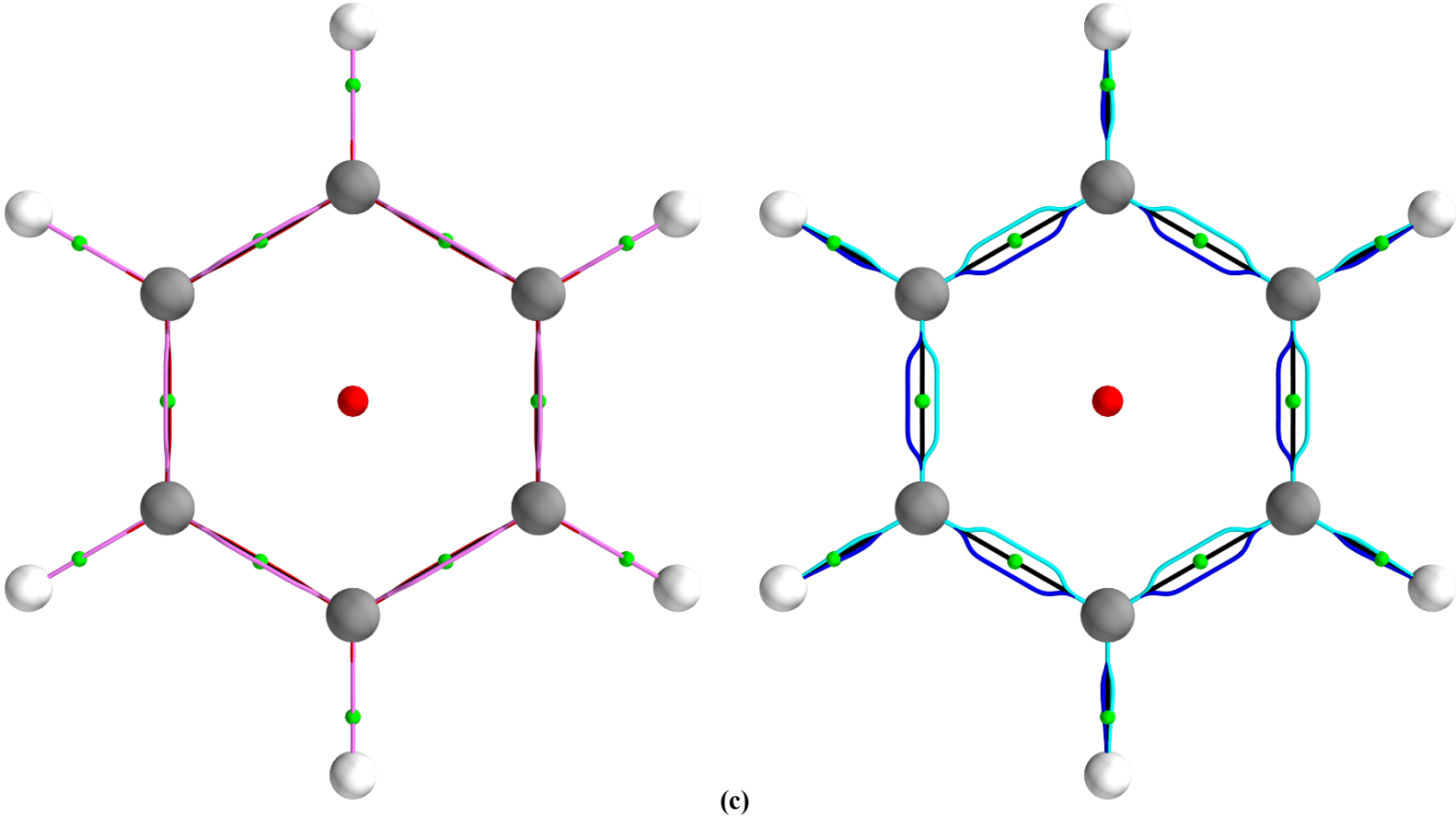

(c)

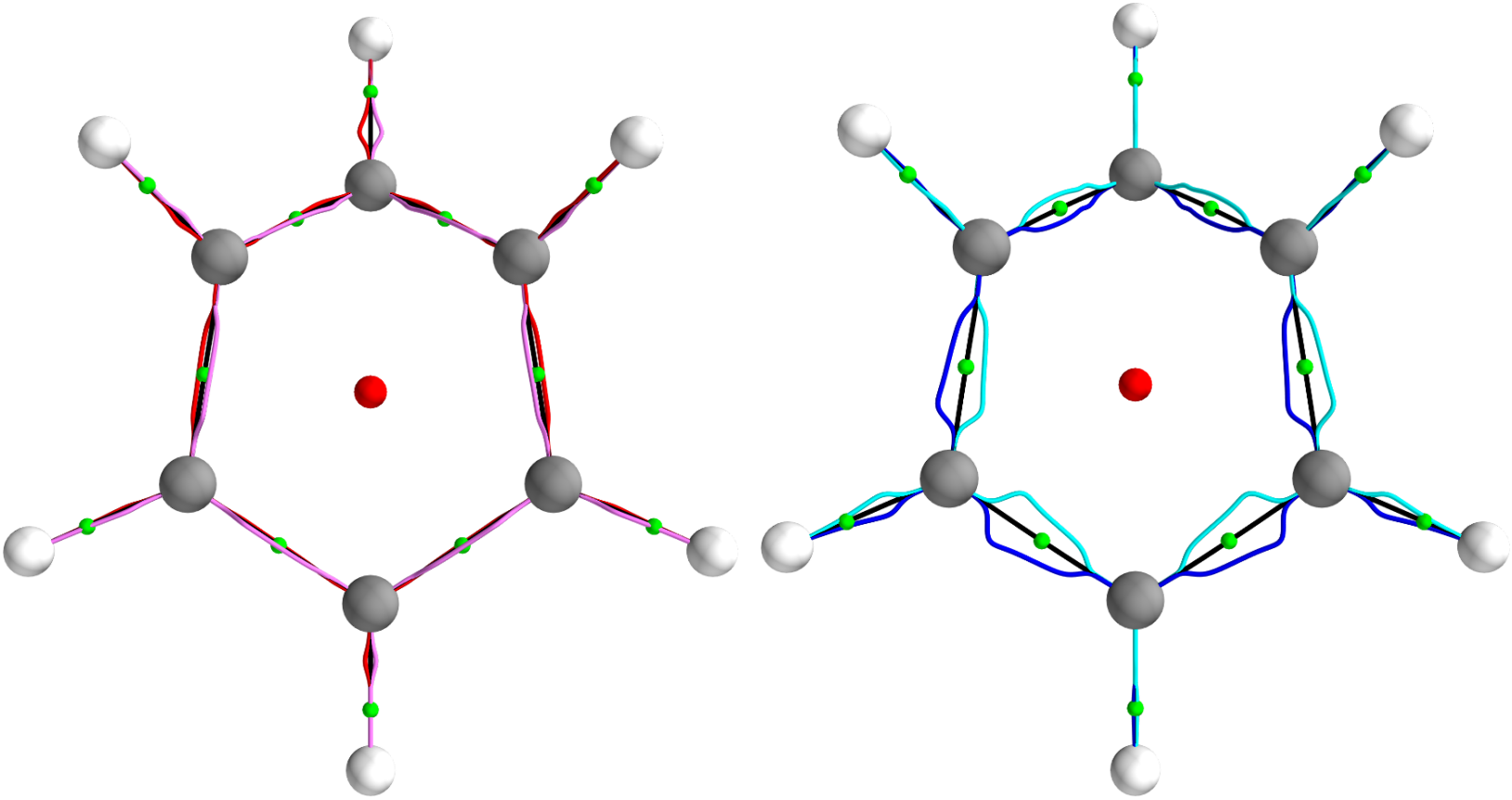

(d)

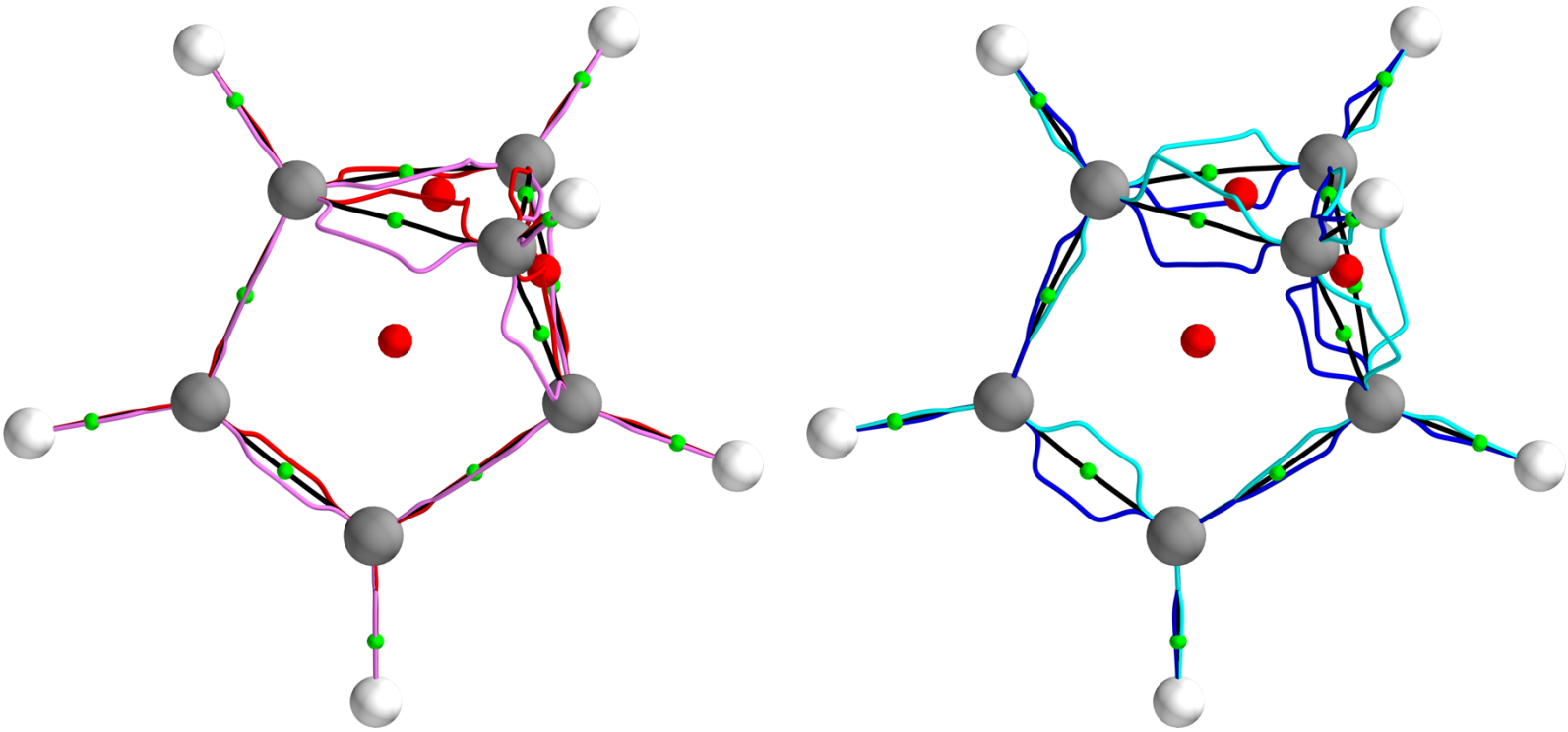

(e)

Figure 1. The bond-path framework set $\mathtt{B}_{0,1}$ = $\{(\boldsymbol{p}_0,\boldsymbol{p}_1),(\boldsymbol{q}_0,\boldsymbol{q}_1),(\boldsymbol{r}_0,\boldsymbol{r}_1)\}$ for benzene S_0, benzene S_1vert, benzene S_1opt and benzvalene S_0/S_1 ConInt and benzvalene S_0 molecular graphs with the $\boldsymbol{q}$(magenta), $\boldsymbol{q}'$(red) and $\boldsymbol{p}$(light-blue), $\boldsymbol{p}'$(dark-blue) paths presented in sub-figures **(a-e)** respectively. The black line indicates the bond-path ($\boldsymbol{r}$) with the undecorated green spheres denoting the positions of the *BCP*s, see **Scheme 2** for the atom labelling.

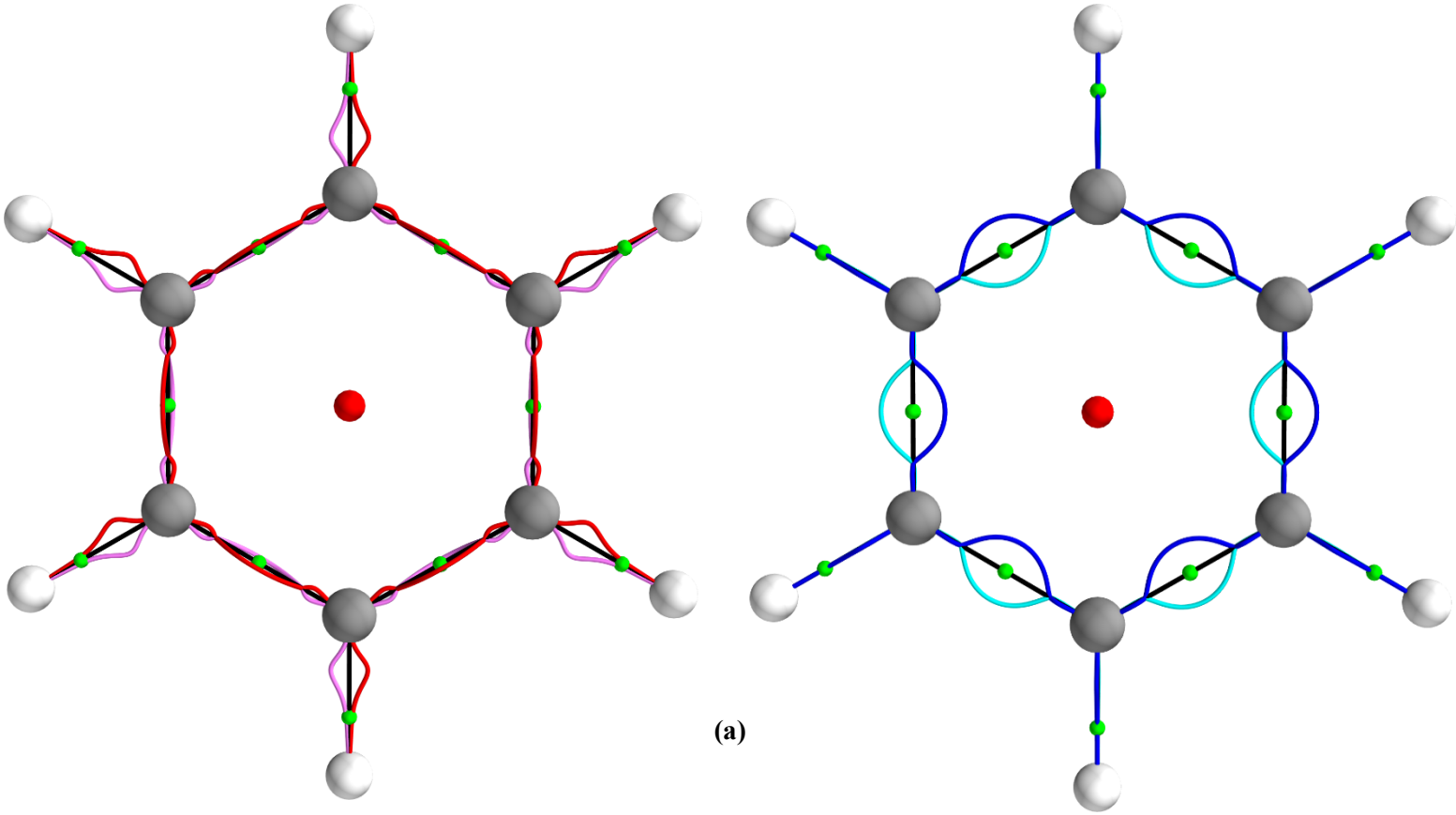

(a)

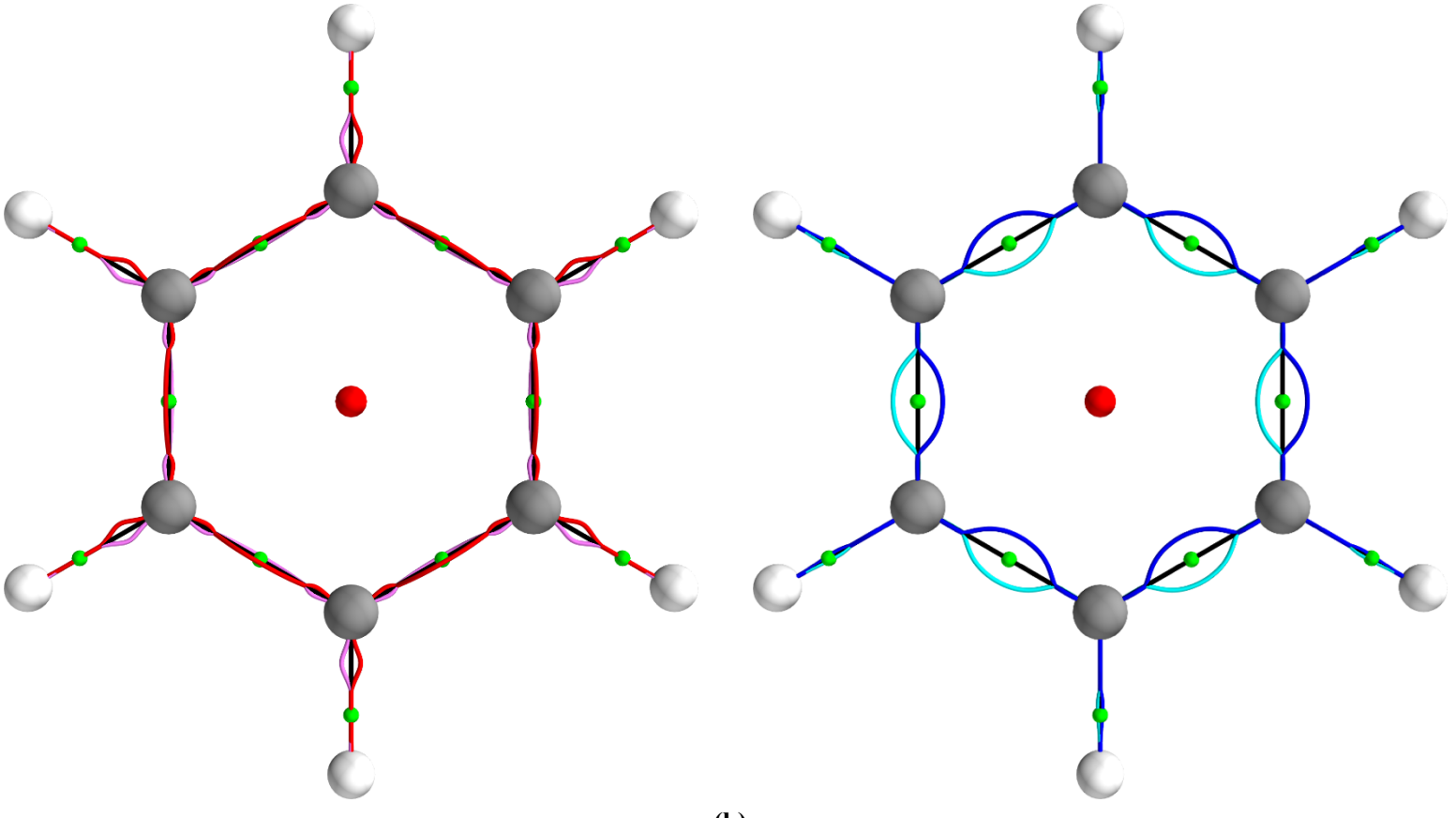

(b)

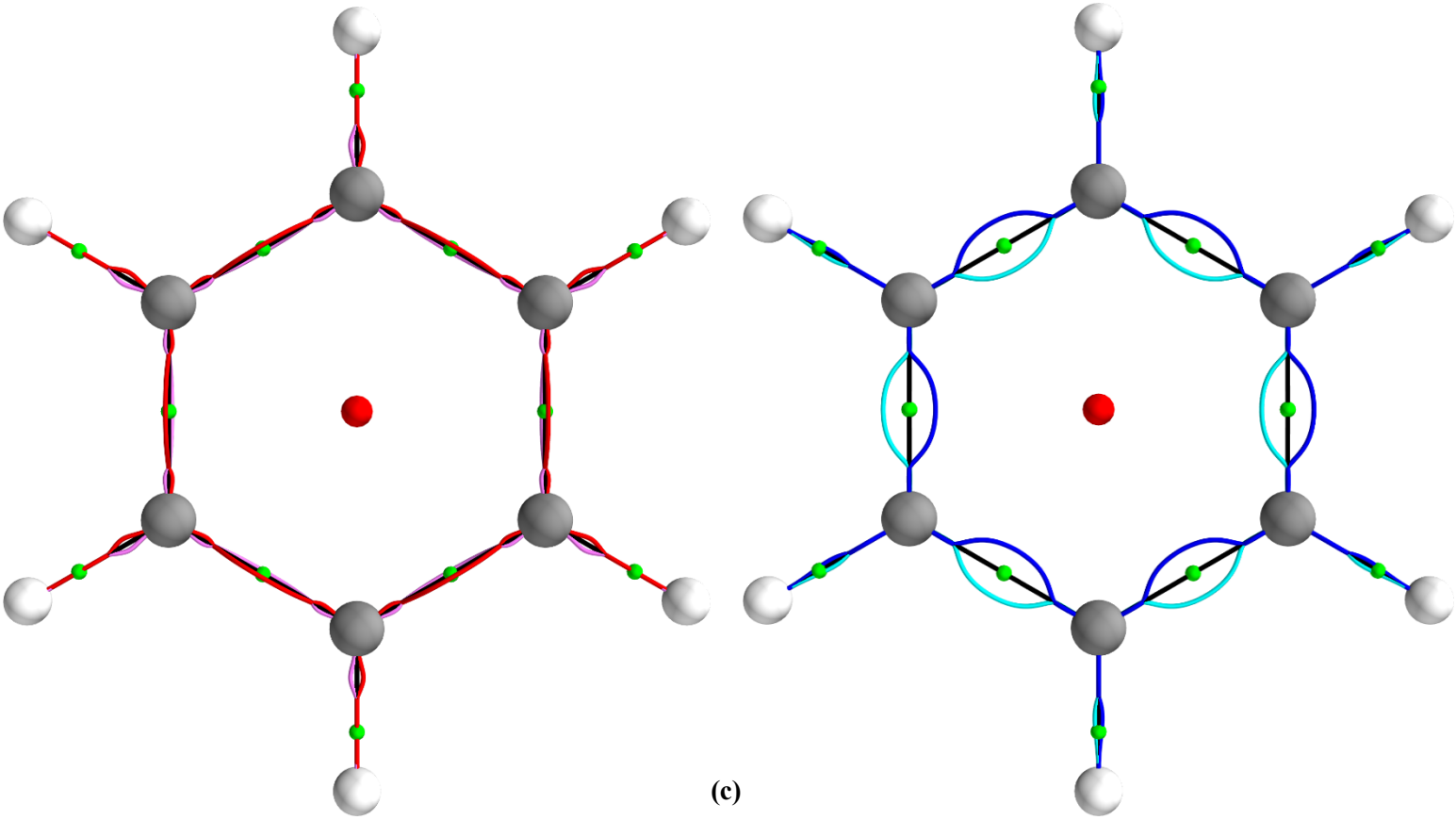

(c)

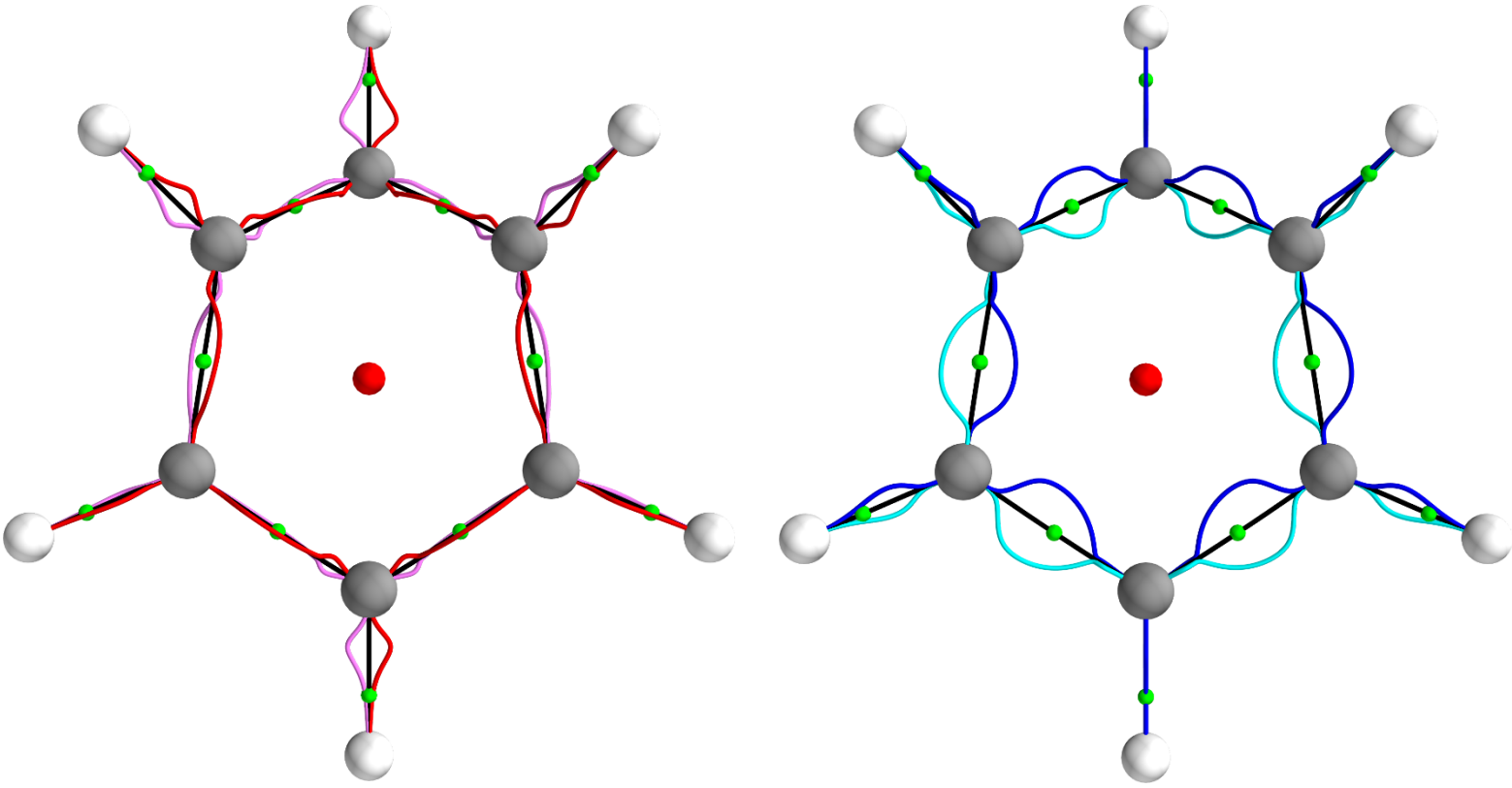

(d)

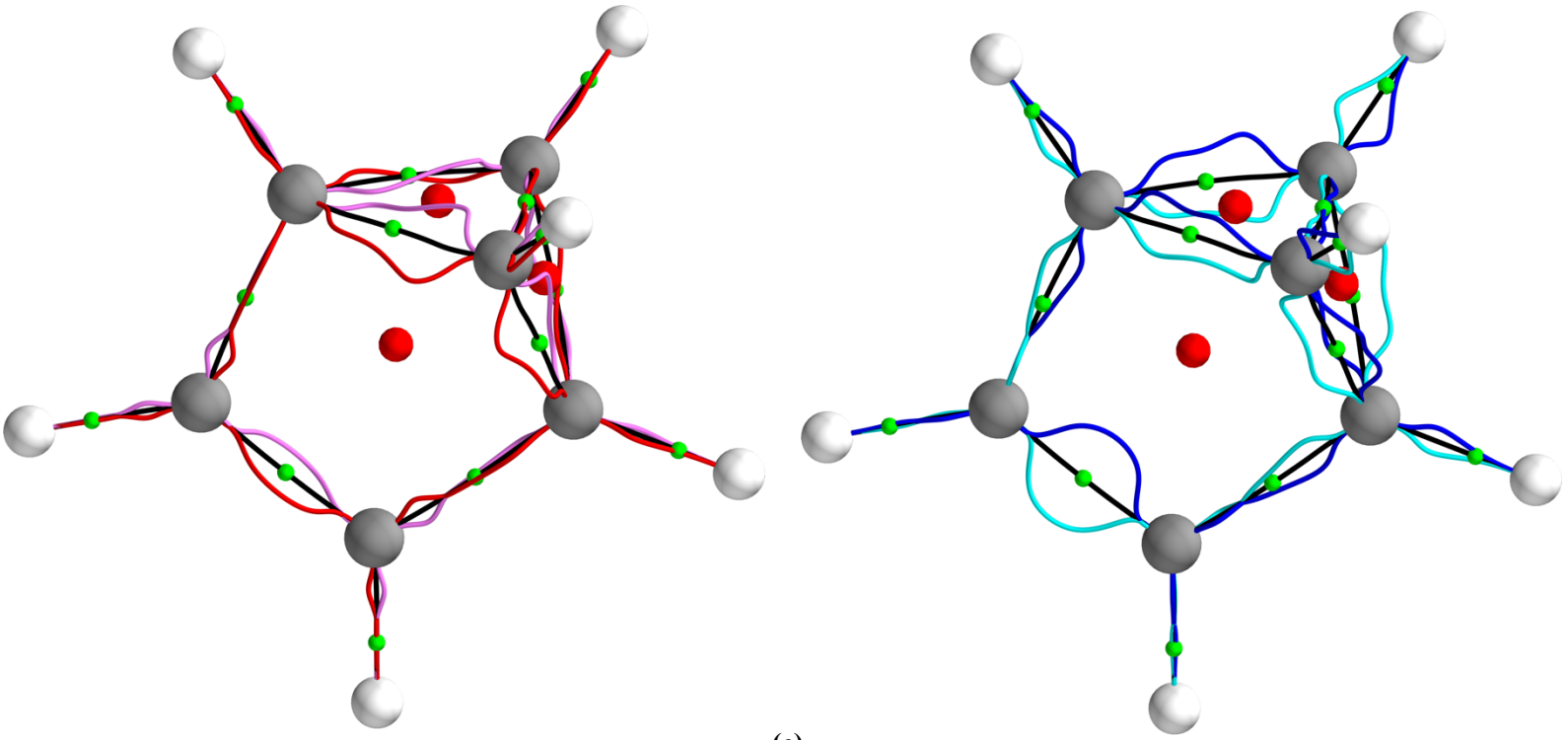

(e)

Figure 2. The stress tensor $B_{\sigma 0,1} = \{(\boldsymbol{p}_{\sigma 0},\boldsymbol{p}_{\sigma 1}),(\boldsymbol{q}_{\sigma 0},\boldsymbol{q}_{\sigma 1}),(\boldsymbol{r}_0,\boldsymbol{r}_1)\}$ for the benzene S_0, benzene S_1 vert and benzene S_1 opt, benzvalene S_0/S_1 ConInt and benzvalene S_0 with $\boldsymbol{q}_\sigma$(magenta), $\boldsymbol{q}'_\sigma$(red) and $\boldsymbol{p}_\sigma$(light-blue), $\boldsymbol{p}'_\sigma$(dark-blue) paths are shown molecular graphs are presented in sub-figures **(a-e)** respectively, with a magnification factor of x5, see the caption of **Scheme 2** for further details.

Conclusions

To summarize, we considered both the scalar and 3-D vector-based measures of bonding that can follow the entire bond-path to better understand the photo-chemical reaction associated with of the formation of benzvalene from benzene. The topological instability of the benzvalene molecular graph was determined using the scalar and vector-based measures to explain the short chemical half-life as the competition between the formation of unstable new bonding that also destabilizes nearest neighbor bonds. The explosive character of benzvalene is indicated by shared-shell *BCP*s that possess the unusual tendency rupture as easily as closed-shell *BCP*s. This is seen from the orientation of the twisted $\{\boldsymbol{q},\boldsymbol{q}'\}$ path-packets, constructed the preferred direction $\underline{\mathbf{e}}_1$ of electronic charge density accumulation, relative to the short *RCP-BCP* lines that is therefore favorable to the coalescence of the associated *BCP* and *RCP*.

The formation of benzvalene from benzene resulted in two additional *shared-shell* C-C *BCPs*, compared with the benzene molecular graph. The formation of additional closed-shell *BCP*s as a result of a reaction process is common and occurs to maximize the bonding density to increase the favorability of a reaction. The formation of shared-shell *BCP*s, in this investigation, is the first time the authors have observed this process. The newly

created shared-shell *BCP*s as well as the *BCP*s in the immediate vicinity are topologically instable. This is evident from the closed-shell *BCP*-like behavior from the scalar measures; very low values of the stiffness S and the vector-based measures, i.e. the direction of the large and twisted $\{\boldsymbol{q},\boldsymbol{q}'\}$ path-packets coinciding with the *RCP-BCP* paths.

In addition, we have demonstrated that for excited state calculations that QTAIM usefully approximates the stress tensor using the stress tensor ellipticity ε_σ version to construct the $\{\boldsymbol{p}_\sigma,\boldsymbol{p}_\sigma'\}$, $\{\boldsymbol{q}_\sigma,\boldsymbol{q}_\sigma'\}$ as opposed to the $\varepsilon_{\sigma H}$ in agreement with investigations only performed in the ground state S_0. The chemical character and high reactivity of the C4-C5 *BCP* is demonstrated.

Work is under development to determine the factors that influence formation in for ground state S_0 and excited states $S_1,...,S_n$, of the bond-path framework set $\mathsf{B}_{0,1,...,n} = \{(\boldsymbol{p}_0,\boldsymbol{p}_1,...\boldsymbol{p}_n), (\boldsymbol{q}_0,\boldsymbol{q}_1,...\boldsymbol{q}_n,), (\boldsymbol{r}_0,\boldsymbol{r}_1,...,\boldsymbol{r}_n)\}$ and the stress tensor $\mathsf{B}_{\sigma 0,1,...n} = \{(\boldsymbol{p}_{\sigma 0},\boldsymbol{p}_{\sigma 1},...,\boldsymbol{p}_{\sigma n}), (\boldsymbol{q}_{\sigma 0},\boldsymbol{q}_{\sigma 1},...,\boldsymbol{q}_{\sigma n}), (\boldsymbol{r}_0,\boldsymbol{r}_1,...,\boldsymbol{r}_n,)\}$ in a wide variety of photo-chemical environments.

This QTAIM analysis provides a strong agreement with insights gleamed from the P_{ij} values which have been shown to provide predictive insight into the formation of the C2-C4 and C1-C3 bonds on the S_0 surface of the conical intersection, a property noted to drive benzvalene formation. P_{ij} analysis has also shown the ability to predict changes in the current carbon bonding framework through the weakening of carbon-carbon couplings upon photoexcitation, and the change in double and single bond character, along with the presence of a three-centre two-electron structure throughout the reaction path on the S_1 surface.

Acknowledgements

The National Natural Science Foundation of China is gratefully acknowledged, project approval number: 21673071. The One Hundred Talents Foundation of Hunan Province is also gratefully acknowledged for the support of S.J. and S.R.K.. M.J.P. thanks the EPSRC for funding through the platform grant EP/P001459/1, while T.M. thanks the EPRSC for support through a DTP studentship.

References:

(1) Katz, T. J.; Wang, E. J.; Acton, N. Benzvalene Synthesis. *J. Am. Chem. Soc.* **1971**, *93* (15), 3782–3783.

(2) Bally, T.; Matzinger, S.; Bednarek, P. The Dewar Benzene Radical Cation and Its Ring-Opening Reaction. *J. Am. Chem. Soc.* **2006**, *128* (24), 7828–7834.

(3) Papadakis, R.; Ottosson, H. The Excited State Antiaromatic Benzene Ring: A Molecular Mr Hyde? *Chem. Soc. Rev.* **2015**, *44* (18), 6472–6493.

(4) Jenkins, S.; Blancafort, L.; Kirk, S. R.; Bearpark, M. J. The Response of the Electronic Structure to Electronic Excitation and Double Bond Torsion in Fulvene: A Combined QTAIM, Stress Tensor and MO Perspective. *Phys. Chem. Chem. Phys.* **2014**, *16* (15), 7115–7126.

(5) Huang, W. J.; Xu, T.; Kirk, S. R.; Filatov, M.; Jenkins, S. QTAIM and Stress Tensor Bond-Path Framework Sets for the Ground and Excited States of Fulvene. *Chemical Physics Letters* **2018**, *713*, 125–131.

(6) Huang, W. J.; Momen, R.; Azizi, A.; Xu, T.; Kirk, S. R.; Filatov, M.; Jenkins, S. Next-Generation Quantum Theory of Atoms in Molecules for the Ground and Excited States of Fulvene. *International Journal of Quantum Chemistry* **2018**, *118* (22), e25768.

(7) Blancafort, L.; Celani, P.; Bearpark, M. J.; Robb, M. A. A Valence-Bond-Based Complete-Active-Space Self-Consistent-Field Method for the Evaluation of Bonding in Organic Molecules. *Theor Chem Acc* **2003**, *110* (2), 92–99.

(8) Ghigo, G.; Moughal Shahi, A. R.; Gagliardi, L.; Solstad, L. M.; Cramer, C. J. Quantum Chemical Characterization of Low-Energy States of Calicene in the Gas Phase and in Solution. *J. Org. Chem.* **2007**, *72* (8), 2823–2831.

(9) Bader, R. F. W. *Atoms in Molecules: A Quantum Theory*; International Series of Monographs on Chemistry; Oxford University Press, USA, 1994.

(10) KUMAR, P. S. V.; RAGHAVENDRA, V.; SUBRAMANIAN, V. Bader's Theory of Atoms in Molecules (AIM) and Its Applications to Chemical Bonding. *J Chem Sci* **2016**, *128* (10), 1527–1536.

(11) Xu, T.; Li, J. H.; Momen, R.; Huang, W. J.; Kirk, S. R.; Shigeta, Y.; Jenkins, S. Chirality–Helicity Equivalence in the S and R Stereoisomers: A Theoretical Insight. *J. Am. Chem. Soc.* **2019**, *141* (13), 5497–5503.

(12) Li, J. H.; Huang, W. J.; Xu, T.; Kirk, S. R.; Jenkins, S. Stress Tensor Eigenvector Following with Next-Generation Quantum Theory of Atoms in Molecules. *International Journal of Quantum Chemistry* **2019**, *119* (7), e25847.

(13) Jones, T. E.; Eberhart, M. E. The Bond Bundle in Open Systems. *Int. J. Quantum Chem.* **2010**, *110* (8), 1500–1505.

(14) Morgenstern, A.; Wilson, T.; Miorelli, J.; Jones, T.; Eberhart, M. E. In Search of an Intrinsic Chemical Bond. *Computational and Theoretical Chemistry* **2015**, *1053*, 31–37.

(15) Bader, R. F. W. A Bond Path: A Universal Indicator of Bonded Interactions. *J. Phys. Chem. A* **1998**, *102* (37), 7314–7323.

(16) Bader, R. F. W. Bond Paths Are Not Chemical Bonds. *J. Phys. Chem. A* **2009**, *113* (38), 10391–10396.

(17) Ayers, P. W.; Jenkins, S. An Electron-Preceding Perspective on the Deformation of Materials. *J. Chem. Phys.* **2009**, *130* (15), 154104-154104–154111.

(18) Jenkins, S.; Kirk, S. R.; Cote, A. S.; Ross, D. K.; Morrison, I. Dependence of the Normal Modes on the Electronic Structure of Various Phases of Ice as Calculated by Ab Initio Methods. *Can. J. Phys.* **2003**, *81* (1–2), 225-231(7).

(19) Bone, R. G. A.; Bader, R. F. W. Identifying and Analyzing Intermolecular Bonding Interactions in van Der Waals Molecules. *J. Phys. Chem.* **1996**, *100* (26), 10892–10911.

(20) Maza, J. R.; Jenkins, S.; Kirk, S. R. 11-Cis Retinal Torsion: A QTAIM and Stress Tensor Analysis of the S1 Excited State. *Chemical Physics Letters* **2016**, *652*, 112–116.

(21) Jenkins, S.; Maza, J. R.; Xu, T.; Jiajun, D.; Kirk, S. R. Biphenyl: A Stress Tensor and Vector-Based Perspective Explored within the Quantum Theory of Atoms in Molecules. *International Journal of Quantum Chemistry* **2015**, *115* (23), 1678–1690.

(22) Kraka, E.; Cremer, D. Description of Chemical Reactions in Terms of the Properties of the Electron Density. *Journal of Molecular Structure: THEOCHEM* **1992**, *255*, 189–206.

(23) Guevara-García, A.; Echegaray, E.; Toro-Labbe, A.; Jenkins, S.; Kirk, S. R.; Ayers, P. W. Pointing the Way to the Products? Comparison of the Stress Tensor and the Second-Derivative Tensor of the Electron Density. *J. Chem. Phys.* **2011**, *134* (23), 234106–234114.

(24) Jenkins, S.; Kirk, S. R.; Guevara-García, A.; Ayers, P. W.; Echegaray, E.; Toro-Labbe, A. Electronic Stress as a Guiding Force for Chemical Bonding. In *Electronic Effects in Organic Chemistry*; Kirchner, R., Ed.; Topics in Current Chemistry; Springer Berlin Heidelberg, 2011; pp 103–124.

(25) Bader, R. F. W. Quantum Topology of Molecular Charge Distributions. III. The Mechanics of an Atom in a Molecule. *The Journal of Chemical Physics* **1980**, *73* (6), 2871–2883.

(26) Bader, R. F. W.; Nguyen-Dang, T. T. Quantum Theory of Atoms in Molecules–Dalton Revisited. In *Advances in Quantum Chemistry*; Per-Olov Löwdin, Ed.; Academic Press, 1981; Vol. Volume 14, pp 63–124.

(27) Wang, L.; Huan, G.; Momen, R.; Azizi, A.; Xu, T.; Kirk, S. R.; Filatov, M.; Jenkins, S. QTAIM and Stress Tensor Characterization of Intramolecular Interactions Along Dynamics Trajectories of a Light-Driven Rotary Molecular Motor. *J. Phys. Chem. A* **2017**, *121* (25), 4778–4792.

(28) Jenkins, S.; Heggie, M. I. Quantitative Analysis of Bonding in 90^{o} Partial Dislocation in Diamond. *Journal of Physics: Condensed Matter* **2000**, *12* (49), 10325–10333.

(29) Jenkins, S.; Morrison, I. The Chemical Character of the Intermolecular Bonds of Seven Phases of Ice as Revealed by Ab Initio Calculation of Electron Densities. *Chemical Physics Letters* **2000**, *317* (1–2), 97–102.

(30) Bin, X.; Momen, R.; Xu, T.; Kirk, S. R.; Filatov, M.; Jenkins, S. A 3-D Bonding Perspective of the Factors Influencing the Relative Stability of the S1/S0 Conical Intersections of the Penta-2,4-Dieniminium Cation (PSB3). *International Journal of Quantum Chemistry* **2019**, *119* (11), e25903.

(31) Boys, S. F. Construction of Some Molecular Orbitals to Be Approximately Invariant for Changes from One Molecule to Another. *Rev. Mod. Phys.* **1960**, *32* (2), 296–299.

(32) Paterson, M. J.; Robb, M. A.; Blancafort, L.; DeBellis, A. D. Mechanism of an Exceptional Class of Photostabilizers: A Seam of Conical Intersection Parallel to Excited State Intramolecular Proton Transfer (ESIPT) in o-Hydroxyphenyl-(1,3,5)-Triazine. *J. Phys. Chem. A* **2005**, *109* (33), 7527–7537.

(33) Paterson, M. J.; Robb, M. A.; Blancafort, L.; DeBellis, A. D. Theoretical Study of Benzotriazole UV Photostability: Ultrafast Deactivation through Coupled Proton and Electron Transfer Triggered by a Charge-Transfer State. *J. Am. Chem. Soc.* **2004**, *126* (9), 2912–2922.

(34) Keith, T. A. *AIMAll, Revision 17.01.25*; TK Gristmill Software: Overland Park KS, USA, 2017.

(35) Ramachandran, P.; Varoquaux, G. Mayavi: 3D Visualization of Scientific Data. *Computing in Science Engineering* **2011**, *13* (2), 40–51.

(36) Robb, M. A.; Garavelli, M.; Olivucci, M.; Bernardi, F. A Computational Strategy for Organic Photochemistry. In *Reviews in Computational Chemistry*; John Wiley & Sons, Ltd, 2007; pp 87–146.

Stress Tensor Eigenvector Following with Next-Generation Quantum Theory of Atoms in Molecules: Excited State Photochemical Reaction Path from Benzene to Benzvalene

Thomas Malcomson[1], Alireza Azizi[2], Roya Momen[2], Tianlv Xu[2], Steven R. Kirk[*2], Martin J. Paterson[1], Samantha Jenkins[*2]

[1]Institute of Chemical Sciences, School of Engineering and Physical Sciences, Heriot-Watt University, Edinburgh, EH14 4AS, UK

[2]Key Laboratory of Chemical Biology and Traditional Chinese Medicine Research and Key Laboratory of Resource National and Local Joint Engineering Laboratory for New Petro-chemical Materials and Fine Utilization of Resources, College of Chemistry and Chemical Engineering, Hunan Normal University, Changsha, Hunan 410081, China

email: steven.kirk@cantab.net
email: samanthajsuman@gmail.com